ELSEVIER

Earth and Planetary Science Letters 165 (1999) 55–66

EPSL

The influence of olivine metastability on the dynamics of subduction

Harro Schmeling [a,*], Ralf Monz [a], David C. Rubie [b]

[a] *Institut für Meteorologie und Geophysik, University Frankfurt, Feldbergstr. 47, D 60323 Frankfurt, Germany*
[b] *Bayerisches Geoinstitut, University Bayreuth, 95440 Bayreuth, Germany*

Received 17 July 1998; accepted 21 October 1998

Abstract

Both seismological observations and mineral physics experiments suggest that old and cold subducting slabs might contain a wedge of metastable olivine ('MO'). Dynamically consistent models of subducting slabs, in which the kinetics of the olivine to spinel (wadsleyite or ringwoodite) transition is treated in a simplified way, are carried out to evaluate the buoyancy effect of MO on the subduction velocity. Assuming slab thicknesses according to the cooling half-space model, we find that MO forms in slabs with ages greater than approximately 70 Myr, and that a significant slowing down of subduction velocity occurs for ages greater than 100 Myr. Because a decrease in the subduction velocity for old lithospheric ages is not observed, our models suggest that the amount of MO in slabs is less than approximately 5000 km^2 in cross section, and that for old lithosphere the cooling half-space model is not applicable.

Keywords: subduction; olivine; spinel; phase transitions; deep-focus earthquakes; thermodynamic properties

1. Introduction

It has long been recognized that the occurrence of deep focus earthquakes shows a strong correlation with the age of the lithosphere at subduction zones and with the thermal parameter ϕ (= product of vertical subduction velocity and age of the lithosphere) (e.g. [1,2]). Extrapolations of the results of high pressure laboratory experiments suggest that the transformation of olivine to spinel (wadsleyite or ringwoodite) is kinetically retarded at temperatures below 600–700ºC, and metastable olivine ('MO') might therefore exist on geological time scales (e.g. [3,4]). Based on laboratory observations of faulting associated with the phase transformation of metastable phases (e.g. [5]) the distribution of deep focus earthquakes may therefore indicate the existence of MO in the mantle. Direct observations of a MO-wedge within cold slabs are not yet conclusive. For example, Iidaka and Suetsugu [6] observed a depressed '410'-seismic discontinuity in Izu-Bonin, while Roecker [7] reported an elevated discontinuity. For the Tonga trench Koper et al. [8] found a slightly better fit of high resolution travel time data if they account for a MO-wedge, but they also showed that this improvement is statistically not significant. Indirect evidence for a MO-wedge is based on deep

* Corresponding author.
E-mail: schmeling@geophysik.uni-frankfurt.de

0012-821X/99/$ – see front matter
PII: S0012-821X(98)00249-0

double seismic zones (e.g. [9]) or seismic anisotropy, which has been explained by en echelon arrays of spinel-filled anti-cracks within the MO-wedge [10].

Because MO has a lower density in the transition zone than the surrounding high-pressure spinel phases, wadsleyite (β-phase) and ringwoodite (γ-phase), buoyancy forces will occur which might lead to observable effects. For example, based on prescribed subduction velocities, Ito and Sato [11] calculated buoyancy forces of slabs which contained MO and concluded that steep slabs may not penetrate into the lower mantle. The buoyancy forces also produce stress fields which may play an important role in producing deep-focus earthquakes [12–14]. The purpose of this paper is to investigate the buoyancy effect of MO on the dynamics and velocity of subducting slabs. It will be shown that the strong negative buoyancy forces associated with old, cold slabs can be significantly reduced by the existence MO. From our models we can impose constraints on the volumes of MO-wedges in old subducting slabs.

2. The model

A dynamically self-consistent model of a subducting slab is calculated by solving the equations of conservation of mass, momentum and energy in the extended Boussinesq approximation (e.g. [15]). Here 'self consistent' means that subduction is driven solely by buoyancy forces due to temperature variations and the density contrast between olivine and the stable transition zone phases, wadsleyite and ringwoodite. For simplicity, we do not distinguish between wadsleyite and ringwoodite, which hereafter are referred to as 'spinel', because the density difference between these phases is small. In the mantle, the density above the olivine–spinel phase boundary is taken as 3400 kg m^{-3} and the density below the transition is taken as 3680 kg m^{-3}. In regions of partial transformation, the density is assumed to increase linearly with spinel fraction. Densities within slabs are higher because of low temperatures and are modelled using a coefficient of thermal expansion of 3.7×10^{-5} K^{-1}.

In two dimensions the momentum equation is given in the stream function formulation (all quantities are non-dimensional, see e.g. [16] for non-dimensionalization):

$$\left(\frac{\partial^2}{\partial x^2}-\frac{\partial^2}{\partial z^2}\right)\eta\left(\frac{\partial^2\psi}{\partial x^2}-\frac{\partial^2\psi}{\partial z^2}\right)+4\frac{\partial^2}{\partial x\partial z}\eta\frac{\partial^2\psi}{\partial x\partial z} = Ra\frac{\partial T}{\partial x}-Rc\frac{\partial\beta}{\partial x} \quad (1)$$

where x, z are the horizontal and vertical coordinates, η is the dynamic viscosity, ψ is the stream function, which is defined by the horizontal and vertical velocity components $v_x = \partial\psi/\partial z$ and $v_z = -\partial\psi/\partial x$, T is the temperature and β is the fraction of spinel. The thermal and compositional Rayleigh numbers are defined as

$$Ra = \frac{\alpha\rho_0 g\Delta T h^3}{\kappa\eta_0}, \qquad Rc = \frac{\Delta\rho g h^3}{\kappa\eta_0} \quad (2)$$

where α is the thermal expansivity, ρ_0 is the reference density, g is the gravitational acceleration, ΔT is a scaling temperature, h is the thickness of the model, κ is the thermal diffusivity, η_0 is the reference viscosity, and $\Delta\rho$ is the density difference between the spinel and olivine phase. The heat equation is given by

$$\left(1+L\frac{\partial\beta}{\partial T}\right)\left(\frac{\partial T}{\partial t}+\vec{v}\cdot\nabla T\right) = \nabla^2 T - v_z\left(\mathrm{Di}\,T_{\mathrm{abs}}+L\frac{\partial\beta}{\partial z}\right)+\frac{\mathrm{Di}}{Ra}\sigma_{ij}\frac{\partial v_i}{\partial x_j} \quad (3)$$

where $L = c_p^{-1}\Delta T^{-1}(a+bz)$ is the non-dimensional, depth-dependent latent heat of the olivine to spinel transformation [4], a and b are constants, c_p is the specific heat, t is the time, $\mathrm{Di} = \alpha g h/c_p$ is the dissipation number, T_{abs} is the non-dimensional absolute temperature, and σ_{ij} is the stress tensor. The terms on the left hand side describe the rate of change of heat due to temperature change and advection, the first term on the right hand side represents heat conduction, the terms containing Di describe adiabatic and dissipative heating, and those containing L account for latent heat release. In this formulation the release of latent heat during phase transformation can be regarded as a reduction of the effective heat capacity (second term within left parentheses on the left hand side) and an increase of adiabatic gradient (second term within parentheses on the right hand side). For an exothermic phase transition (where $L < 0$)

numerical stability is retained as long as the first parenthesis in Eq. 3 remains positive.

The viscosity is assumed to be temperature, pressure and stress dependent according to the dislocation creep law of olivine single crystals [17,15]. This law is given as a superposition of two strain rates, $\dot{e} = \dot{e}_1 + \dot{e}_2$. Each component is described by an empirical exponential law,

$$\dot{e}_i = D_i \Delta\sigma^{n_i} \tag{4}$$

where $\Delta\sigma$ is the difference between maximum and minimum stress, n_i is the power law exponent, and D_i is a diffusion term with

$$D_i = A_i P_{O_2}^{m_i} \exp\left(-\frac{E_i + PV_i}{RT}\right) \tag{5}$$

which depends on the oxygen fugacity P_{O_2}, which is given by

$$\log_{10}(P_{O_2}/\text{atm}) = F_1 + \frac{F_2}{T} + F_3\frac{P/\text{atm} - 1}{T} \tag{6}$$

Here A_i is a constant, m_i is an exponent, E_i is the activation energy, P is the pressure, V_i is the activation volume, and R is the gas constant. The values used are listed in Table 1.

Within the upper few tens of kilometres, a depth-dependent plastic rheology is superimposed by a rheology based on frictional sliding, described by Byerlee's law, in order to account for the weakening effect of a cold brittle upper lithosphere. At the upper left corner of the model a localized weak zone is assumed to decouple the lithosphere from the side wall and allow it to move freely. This weak zone is intended to mimic a mid-ocean ridge. The range of viscosity variations within the model is restricted to 10^{21} Pa s $< \eta < 10^{27}$ Pa s. This allows the formation of a highly viscous lid, which may bend and deform during subduction in a self consistent way due to dislocation creep. The lower value of 10^{21} Pa s is usually reached within the asthenospheric mantle and has been chosen to represent the average upper mantle viscosity.

Rather than explicitly solving the kinetic equations of the phase transformation a simplified kinetic phase diagram is used to model the transformation of olivine to spinel (Fig. 1; cf. [4]). The 1% and 99% lines separate the olivine and spinel regimes. The vertical line segments separating metastable olivine from spinel represent the disequilibrium phase transformation at low temperatures. Although during the disequilibrium transformation the fraction of spinel is expected to increase exponentially or even over-exponentially with temperature and time [4,18], for simplicity we assume only a linear increase with temperature. This simplification may give an inadequate picture of the detailed structure of the boundary of the MO-wedge, particularly because the feedback mechanism between the release of latent heat and the kinetics of the phase transformation [19,20] is neglected. However, we believe that the general shape and volume of the MO-wedge will be modelled correctly and the dynamics of the whole subducting slab will not be affected by this simplification. The depth and slope of the equilibrium transitional region (i.e. the sub-horizontal part of the transition curves at $T > \sim 700$°C) is based on the thermodynamic data for $Mg_{1.8}Fe_{0.2}SiO_4$ of Akaogi et al. [21]. The complete disequilibrium phase transi-

Table 1
The parameters used for calculating the mantle viscosity after [15,17]

Symbol	Value and unit	Meaning
A_1	2.1×10^{-17} Pa^{-n1} atm^{-m1} s^{-1}	Preexponential constant
A_2	5.2×10^{-16} Pa^{-n2} tm^{-m2} s^{-1}	Preexponential constant
$E_1 = E_2$	540 kJ/mol	Activation energy
$V_1 = V_2$	15×10^{-6} m^3/mol	Activation volume
$n_1 = n_2$	3.5	Power law exponent
F_1	9	Factor in oxygen fugacity
F_2	2.5738×10^4 K	Factor in oxygen fugacity
F_3	0.092 K	factor in oxygen fugacity
m_1	0.02	Exponent in oxygen fugacity
m_2	0.23	Exponent in oxygen fugacity

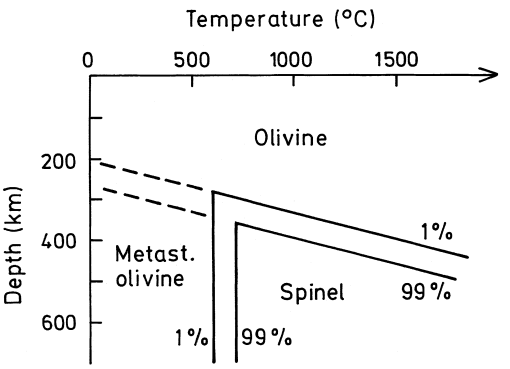

Fig. 1. Simplified disequilibrium (kinetic) phase diagram of the olivine–spinel transition as used in the models (cf. [4], fig. 9). Lines of 1% and 99% spinel fraction are shown and indicate the start and completion of the olivine–spinel phase transformation along depth–temperature paths characteristic of subduction zones [4]. The vertical segments of the lines show the conditions required for transformation at low temperature and are consistent with metastable olivine persisting at $T < 600$ºC. At higher temperatures (>700ºC), transformation occurs relatively close to the equilibrium phase boundary. The spinel fraction is assumed to increase linearly between the 1% and 99% lines.

tion is implemented by determining $\beta(T, z)$ according to the diagram in Fig. 1 ($\beta = 0$ in the olivine and metastable olivine field, $\beta = 1$ in the spinel field and $0 < \beta < 1$ between the 1% and 99% lines). These β-values and their derivatives are used when solving Eqs. 1 and 3. Note that the kinetic model used here is based on a model of Rubie and Ross [4] that has large uncertainties and is oversimplified in terms of transformation mechanisms [22,23]. We therefore consider below the effects of uncertainties in the kinetic model on our conclusions.

To initiate subduction and keep it going we follow the approach of Christensen [24]: As initial temperature distribution, a thermal boundary layer representing the oceanic lithosphere of pre-defined thickness is assumed within the left part ($0 \leq x \leq 2010$ km) of the model (Fig. 2, top). In the mantle below, an adiabatic temperature distribution is assumed, which intersects the olivine–spinel boundary at a depth of 410 km at 1600ºC in accordance with thermodynamic data of Akaogi et al. [21]. Due to latent heat, a temperature jump of 50ºC is assumed at that depth. In the remaining 670 km of the model (2010 km $< x \leq 2680$ km) no thermal boundary layer (i.e. no lithosphere) is assumed and the adiabatic temperature distribution reaches to the surface. Although the absence of an overriding plate may be unrealistic, an overriding plate exerts forces on the slab that are difficult to model in a fluid dynamical model such as the one presented here and do not fall within the scope of this paper. We assume that these forces are small compared to slab pull forces. The assumed temperature distribution can be regarded as a possible end member of a back arc basin with very thin lithosphere. To initiate subduction, an initial ridge push force is generated by locally elevating the initial temperatures of the mantle close to the left edge of the lid (see Fig. 2, top).

Further boundary conditions are free slip at all boundaries, thermally insulating sides and a bottom heat flux of 20 mW/m^2. Due to computational limitations the depth of the model is restricted to 670 km and the aspect ratio is 4. This model configuration implies that slabs cannot penetrate into the lower mantle.

The equations are solved on a 241×61 grid for the stream function, viscosity and spinel fraction and a 481×121 grid for the temperature using a finite difference code FDCON developed by one of us (H.S.). This resolution is sufficient to adequately model the large scale dynamics of a subducting slab including buoyancy effects of MO. However, small scale features like the fine structure of the MO-wedge resulting from the non-linear coupling between metastability, temperature, stress, and rheology [25,14] cannot be resolved.

3. Results

First the behaviour of a typical subduction model will be presented and then the dependence on age will be investigated. Fig. 2 shows the evolution of a subducting slab at different times, while Fig. 3 (solid curve) shows the absolute value of velocity of a characteristic tracer within the slab as a function of time. This tracer had an initial position at $x = 1270$ km (i.e. 740 km left of the slab edge) and represents the subducting part of the slab at a later stage of evolution. The initial thickness of the slab corresponds to a 111-Myr old lithosphere. After a period of 24 Myr of slow acceleration with velocities below 1 cm/a the slab speeds up and subducts. After 27 Myr

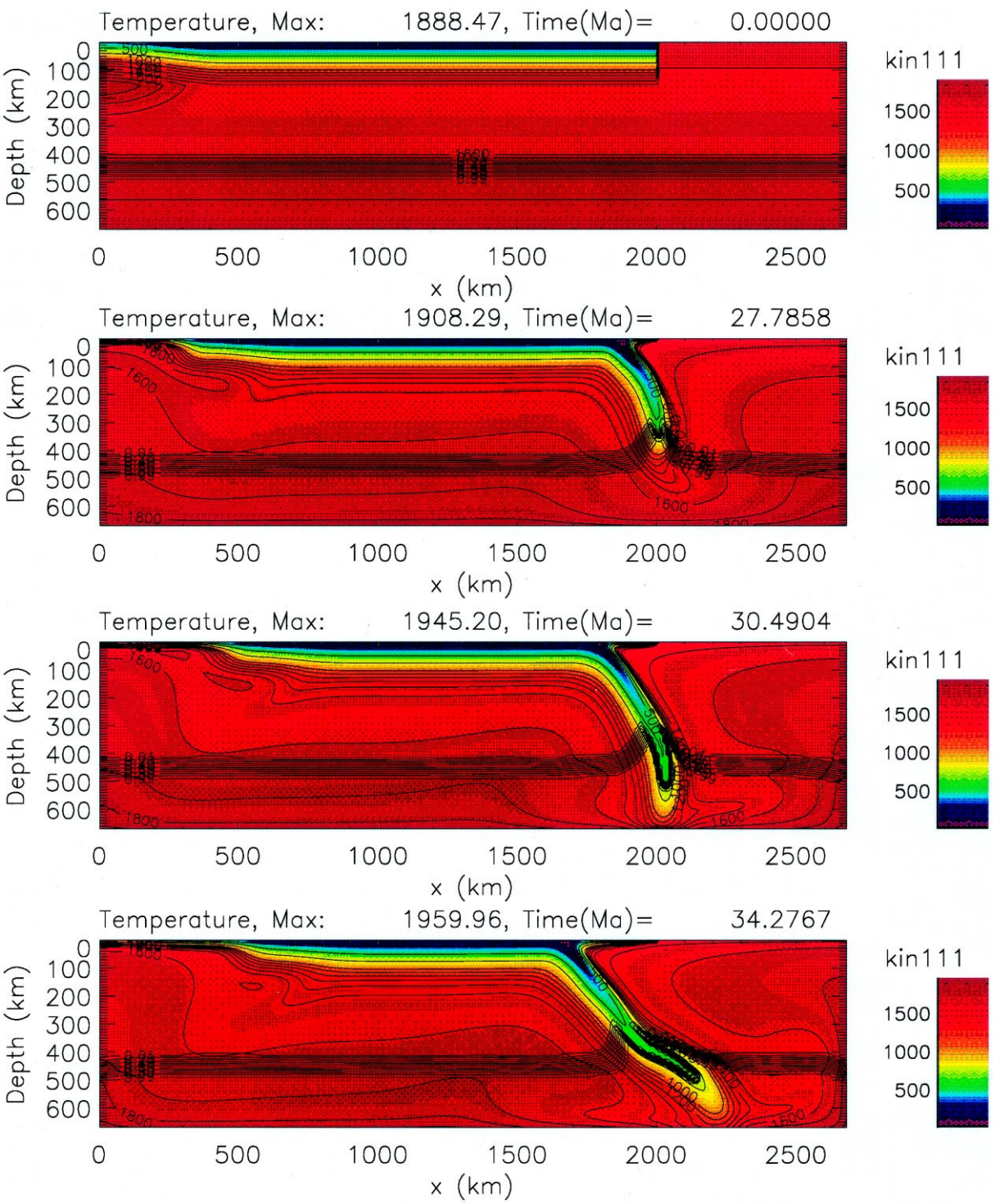

Fig. 2. Evolution of a subducting slab with time from top to bottom. Initial thickness of slab was chosen corresponding to a 111-Myr old lithosphere. Colours and a few contour lines represent temperature. The dense set of contour lines between 400 and 500 km depth represent the transition from olivine to spinel, and give the fraction of spinel.

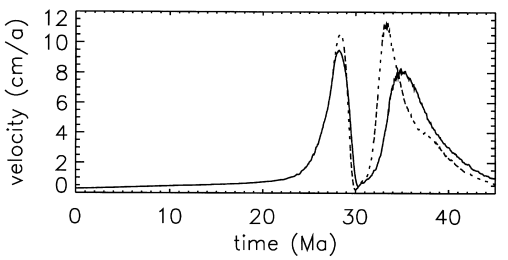

Fig. 3. Absolute value of velocity of a tracer situated within the subducting slab. Initial position of the tracer is 740 km left of the front of the slab. The full curve gives the velocity of the slab in which MO is present, the dashed curve represents a slab of same age and thickness, but without MO.

it reaches the olivine–spinel equilibrium boundary which is strongly deflected upwards by then. Sinking velocities at that stage are of the order of 10 cm/a. Because the interior of the slab is still sufficiently cold, the olivine–spinel transformation is retarded and a MO-wedge develops. Upon encountering the bottom of the box (which mimics an 'impermeable spinel–perovskite boundary'), subduction slows down at 30 Myr. If the slab were allowed to penetrate the spinel–perovskite boundary, it would still slow down, but to a lesser extent. The frontal part of the slab is still stiff and needs time to bend again. During a second phase of acceleration (Fig. 2, bottom, and Fig. 3) the lower part of the slab moves towards the right hand side of the box, while the trench migrates towards the left. As the subducted slab reaches the side of the model box, it cannot leave the box and further subduction is slowed down.

For comparison, the same model has been calculated assuming thermodynamic equilibrium between olivine and spinel even at low temperatures, i.e. suppressing the formation of MO. As a result, the olivine–spinel transition is elevated similarly as in Fig. 2, however, without forming a MO-wedge. Therefore, the negative buoyancy forces due to low slab temperatures and the elevated olivine–spinel phase boundary are larger and the subducting velocity is higher (dashed curve in Fig. 3). This increase in velocity is not very strong during the first subduction peak at 28 Myr, because the MO-wedge is not fully developed during this transient stage. At the time 33 Myr, which represents ongoing subduction at a more mature stage, the second peak is significantly higher compared to subduction with MO. If the slab were allowed to penetrate into the lower mantle, the second peaks would be higher and last longer, however, the difference between them is expected to remain similar.

To investigate the effect of MO for slabs of different thicknesses or ages, a series of models has been calculated with varying initial thicknesses of the lithosphere. Applying the cooling half-space model the initial thicknesses correspond to ages of 5, 33, 49, 70, 90, 111, 131, and 165 Myr. The general behaviour of these models is similar to that shown in Fig. 2 and Fig. 3. In Fig. 4 we show close ups of the subducting slab of three of these models at comparable times (i.e. during the second peak of the slab velocity, cf. Fig. 3). The initial ages of the slabs are 33 Myr (top), 70 Myr (middle), and 111 Myr (bottom). Clearly a transition from a slab without MO to one containing a well developed MO-wedge can be seen. It should be noted that the total ages of the slabs have to be taken as the initial ages plus the model time, which varies between 30 and 34 Myr.

To quantify the amount of MO, Fig. 5 shows the increase in cross sectional area in km^2 of MO for these models. Again, the numbers near the curves give the initial ages of the lithosphere. It can be seen that, despite the larger negative thermal buoyancy, subduction is delayed for old and thick lithospheres. This is due to the increased stiffness of old lithosphere. Younger lithospheres are not able to produce large amounts of MO. For example, the 33-Myr lithosphere subducts after a model time of 25 Myr and does not form any MO during this first stage. Upon continued subduction that slab becomes older and subsequently produces small amounts of MO at 42 Myr and a larger amount at 57 Myr of model time. The oscillations seen in Fig. 5 indicate the time-dependent nature of subduction inherent in our models, while the gradual decrease in MO-volume for greater times results from diffusive warming of the subducted slab.

Fig. 4. Close ups of subducting slabs of different initial ages during the second velocity peak (cf. Fig. 3). The initial ages and the model times of the snap shots are 33 and 30.1 Myr (top), 70 and 30.3 Myr (middle), and 111 and 34.3 Myr (bottom), respectively.

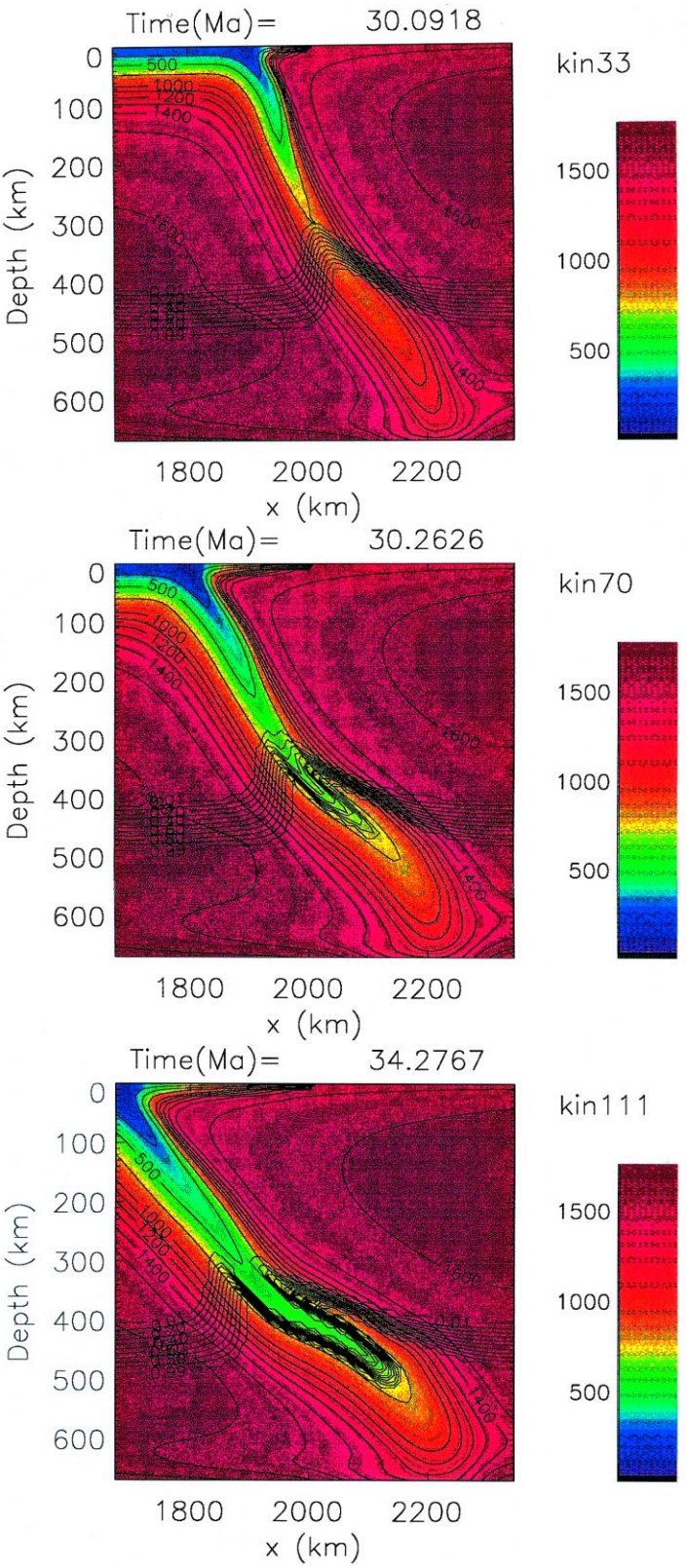
Time(Ma)= 30.0918
kin33
Depth (km)
0
100
200
300
400
500
600
1800
2000
2200
x (km)
1500
1000
500
Time(Ma)= 30.2626
kin70
Time(Ma)= 34.2767
kin111

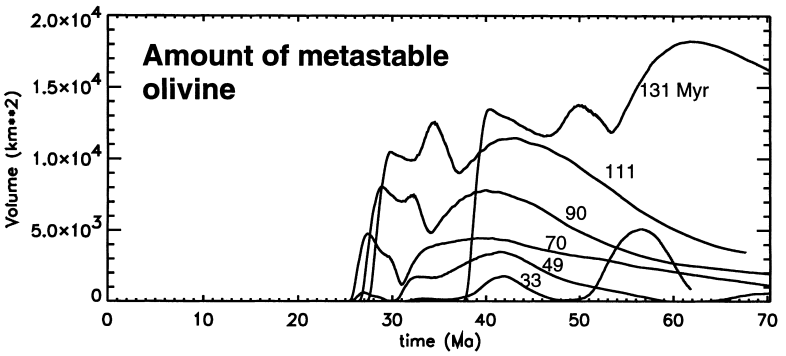

Fig. 5. The amount of metastable olivine in km^2 for the different models as a function of time. The ages beside the curves give the initial age of the lithosphere before subduction.

The effect of MO on slab velocities during ongoing subduction is shown in Fig. 6. The velocities represent the peak velocity of the second peak of each model (cf. Fig. 3). Both model sets with and without MO development are shown. For young lithospheres (<90 Myr) slab velocities increase approximately linearly with lithospheric thickness (which is proportional to the square root of the age). Above 90 Myr slabs without metastable olivine still show a slight increase in velocity except for the oldest slab. The decrease of the slope of the velocity curve is a consequence of the increasing stiffness of the slab, which counteracts the driving effect of negative buoyancy. Clearly the effect of the buoyant MO-wedge is seen for ages greater than 80 Myr because slab velocities decrease sharply with age. Thick and cold slabs are slowed down by up to 30% compared to slabs of the same age but without MO. A qualitatively similar result has recently been found by Marton et al. [26] who calculated slab velocities by balancing buoyancy and drag forces in a simplified slab model. Inspection of Fig. 5 shows that the slabs with ages at the trench of 64 and 79 Myr (initial slab ages 33 and 49 Myr, respectively) contain already small amounts of MO, however, the slab velocities are only slightly affected. Only MO-amounts with a cross-sectional area of more than 5000 km^2 have a significant effect on slab velocities.

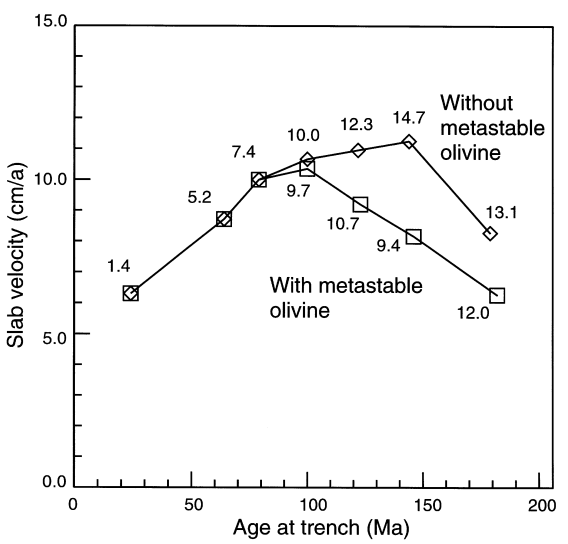

Fig. 6. Slab velocity during subduction of slabs with different ages at the trench. Squares represent models in which metastable olivine may be formed, diamonds show models in which metastable olivine is not allowed to form. The velocity is given as the absolute value of velocity of a tracer within the downgoing part of the slab. The numbers beside the symbols give the thermal parameter of the slab (vertical velocity times age at trench) in units of 1000 km. The age at trench is taken as the initial slab age plus the model time of the second velocity peak (cf. Fig. 3). The initial slab ages of the models are (corresponding to the symbols from left to right): 5, 33, 49, 70, 111, 131 Myr.

The numbers beside the symbols in Fig. 6 give the thermal parameter ϕ of the slabs of the model slabs in units of 1000 km. Although small amounts of MO are formed already for ϕ-values of 5200 and 7400 km, significant amounts of MO (>2000 km^2) occur only for values of ϕ above 7400 km. For the models without MO, ϕ increases up to 14,700 km, while in the models with MO ϕ does not rise significantly above 10,000 km. Obviously, MO slows down the slabs in a self-regulating manner keeping ϕ close to 10,000 km. This effect, which has

previously been discussed by Bassett [27] and Rubie [28], was termed the "parachute effect" by Kirby et al. [2]. It should, however, be noted, that due to numerical restrictions (box size) our models are strongly time dependent and we do not obtain steady state subduction. As a consequence, the thermal parameter decreases to very small values after each peak in the rate of subduction, while significant amounts of MO are still present. Thus, previous subduction history and the formation of MO do not always correspond with the actual thermal parameter of a subduction zone.

In our models the disequilibrium phase transformation has been assumed to take place in a temperature range between $T_1 = 600$ºC and $T_2 = 700$ºC. Because the precise values of these temperatures are poorly known, we have also tested different values. Increasing T_1 and T_2 by 100ºC leads to significantly higher amounts of MO, which reduce the slab velocities with increasing age already for ages greater than 80 Myr. For these ages the velocities shown in Fig. 6 decrease roughly by another 1.5 cm/a. Decreasing T_1 and T_2 by 100ºC has the opposite effect. Negligible amounts of MO are present for ages younger than 110 Myr, and even the model with a slab age of 145 Myr is hardly affected.

4. Discussion

4.1. Inferences for subduction zones

Our models suggest that subduction of old and cold lithosphere may produce significant amounts of MO, which should have a considerable effect on the subduction velocities of slabs. A decrease in subduction velocity with age as predicted by the models for ages greater than 100 Myr (Fig. 6) has not been reported so far. Although plate ages near the trench of the western Pacific plate vary between 70 and 180 Myr, there is no trend by which subduction velocities decrease with age. Although the plate behaves rigidly as a single unit allowing only for one particular angular velocity, such a trend should still be visible because different parts of the trench have different and probably independent rates of trench rollback. Thus we have to conclude that in the subduction zones of the western Pacific MO may be present, but not in large volumes (probably less than 5000 km^2 in cross section). These inferred volumes, which might be represented by MO-wedges of 25 km × 200 km size for example, are still sufficiently large to explain most deep focus earthquakes. For slabs older than 100 Myr, volumes less than 5000 km^2 are obtained if the disequilibrium phase transformation takes place between kinetic temperatures of $T_1 = 500$ºC and $T_2 = 600$ºC rather than 600 and 700ºC, respectively. However, these temperatures do not allow for noticeable amounts of MO in slabs younger than 100 Myr. In this case, the occurrence of deep earthquakes would have to be explained by mechanisms other than transformational faulting, at least for some slabs. As an alternative to reducing T_1 and T_2, the lithosphere may not cool any further after reaching an age of about 100 Myr. In this case, T_1 and T_2 might be even higher than the assumed values by up to 100ºC. This second possibility will be discussed further in the following section.

Our models suggest that MO will develop in slabs with a thermal parameter greater than 5400 km, but the slab velocities are not strongly affected by the buoyancy of MO until the thermal parameter becomes as large as approximately 10,000 km. This result is in general agreement, for example, with Kirby et al. [2] who presented a compilation of earthquake depths versus thermal parameter, in which deep earthquakes occur generally only for $f > 5000$ km. A few exceptions include South America (Brazil, Peru, North Argentina, South Bolivia) with $\phi = 3000$ km. As mentioned above, the ϕ-value of a subducting slab may vary strongly with time, and some of our models still have large amounts of MO even though their ϕ-values have decreased significantly. While in our models a decrease of f was mainly due to slowing down of subduction velocities, decreasing ages of subducting plates at migrating trenches might also be important in nature. Either of these effects might be responsible for the small f-values of some South American subduction zones. Our models show also that the thermal parameter will not increase significantly above 10,000 km due to the slowing down effect of MO. These findings are not in agreement with the thermal parameters of some subduction zones (Marianas, Tonga) which are estimated to be significantly larger than 10,000 km (e.g. [2]). However, these estimates are

based on the assumption of steady state velocities of the Pacific plate and of the trench roll back. Any time dependence, e.g. a change of the subduction angle by a few degrees per Myr, as observed also in our models, may change thermal parameters significantly. Therefore, the relation between the maximum earthquake depth and the thermal parameter should be used with caution, as long as the time-dependent history of subduction zones is not known.

Another possibility for MO to be present at smaller ϕ-values than found in this study is to cool the lithosphere more effectively. Thermal models of the lithosphere including a temperature dependent thermal diffusivity show that the central part of the lithosphere (above the 800ºC isotherm) might be colder by up to 100ºC compared to the case of constant thermal diffusivity [29].

4.2. Cooling due to the plate model

Cooling and thickening of the lithosphere may not take place for arbitrarily long times as would be the case for a cooling half-space. For ages greater than 90 Myr a deviation of *bathymetry* from the cooling half-space model is observed (see e.g. [30]) supporting the cooling plate model instead. According to the cooling plate model the lithosphere does not cool and thicken any further, once it has reached an age of 80 to 100 Myr. It should be noted, however, that the deviation from the cooling half space model is not at all clear for the *heat flow* data presented, for example, by Stein [31] or Sclater et al. [32]. They can almost equally well be explained by the cooling half-space model. As discussed above, our results do not favour very cold and thick lithosphere, because we do not see the slowing down effect of the MO. Our models are in agreement with lithospheric plates that have cooled and thickened during the first 100 Myr of their evolution, but have not changed their thermal structures thereafter. Thus, our models provide indirect evidence in support of the cooling plate model.

4.3. Model restrictions and robustness of the conclusions

Our models are restricted to the upper mantle, thus, as the subducted slab approaches the 670 km-discontinuity its lower part is fully supported by the bottom of the box. In case of penetration of the lower mantle, the negative buoyancy of the cold slab would be supported by an upward deflection of the spinel–perovskite boundary and by viscous forces of the lower mantle. If the lower mantle has a higher viscosity than the upper mantle, these forces can be expected to locally balance the negative buoyancy forces. Thus to a first order, we expect that our velocities are not biased too much by the restriction of an impenetrable bottom. Even if the absolute values of the second peaks of our velocities would be different in case of lower mantle penetration, we expect that the difference between the cases with and without MO are not affected significantly. To resolve this question, higher resolution models which also include the spinel–perovskite transition, are needed.

The maximum depths of the MO-wedge do not exceed 550 km in the models presented here. This is mainly due to the influence of the bottom boundary in combination with the high viscosity of the cold slab. Flattening of the slab near the bottom requires some time, allowing the MO to transform into spinel. Rheological weakening of transformed material surrounding the MO-wedge, as suggested by Rubie [33] and Riedel and Karato [25], may aid this bending process allowing the MO to reach somewhat greater depths than found here. Also if the slab would be allowed to penetrate deeper through the spinel–perovskite transition, greater depth extents of the MO-wedge are to be expected.

We do not believe that our conclusion about maximum volume of 5000 km^2 of MO in old slabs is significantly affected by the particular choice of our rheological model parameters. As discussed above, more realistic slab rheologies would weaken the slab even more. In such slabs buoyancy due to large amounts of MO ($>$5000 km^2) would lead to even more pronounced effects on subduction velocity. As an extreme case we have calculated a model of constant viscosity convection with a disequilibrium phase transformation (i.e. no rheological slab at all). In this case MO accumulates directly below 410 km depth and completely inhibits subduction after some time. Another point of concern might be the truncation of the mantle viscosity at 10^{21} Pa s. Models with lower truncation values have been tested, but lead to unrealistically high subduction rates. As long

as our slabs without MO have reasonable subduction velocities, we believe that our conclusions about the dynamic effect of MO are quantitatively correct.

In the extended Boussinesq approximation density is assumed constant except in the buoyancy term of the momentum equation. Assuming a density contrast of 8% between olivine and spinel, this implies that we overestimate the flow velocities below the olivine–spinel transition by approximately the same relative amount. The geometry of the flow field is only slightly affected by this approximation. This can be seen by evaluating the deflection of streamlines at an univariant phase transition, which is given by

$$\tan e = \frac{\rho_{\mathrm{spi}}}{\rho_{\mathrm{ol}}} \tan i \qquad (7)$$

where i and e are the angles between an incoming or emerging streamline and the normal to the phase boundary, and ρ_{ol} and ρ_{spi} are the densities of olivine and spinel, respectively. For the ovine to spinel transition the maximum possible deflection of a streamline due to non-Boussinesq-effects is only 2.2° and is not expected to change our results significantly.

5. Conclusion

For the first time dynamically consistent models of subduction of lithospheric slabs have been calculated, in which buoyancy effects of the olivine–spinel phase change and of metastable olivine (MO) have been included. Assuming a cooling half-space model for the lithosphere, we have tested the subduction behaviour of slabs of different thicknesses or ages. Old and thick slabs develop large amounts of buoyant MO which retard subduction due to the so-called parachute effect [2]. From our models we are able to quantify this effect and observe a significant reduction of subduction velocities for lithospheric ages greater than 90 Myr. This reduction is associated with the development of relatively large amounts of MO (>5000 km^2 in cross section). A further effect of this reduction is to restrict the maximum thermal parameter of subducting plates to values of roughly 10,000 km. We note that if plates do not continue to cool beyond ages greater than 90 Myr (i.e. if the cooling plate model is applicable) no significant buoyancy effect of MO is expected.

Because a significant reduction in subduction velocity is not observed for increasing plate ages in the western Pacific, we conclude from our models that MO may not be present in large volumes and the parachute effect is probably not very important. Smaller amounts (<5000 km^2 in cross section) may well be present and may be responsible for deep focus earthquakes but they do not lead to a first order observable effect in subduction dynamics. To fully resolve this question high resolution models are necessary which also take into account the spinel–perovskite transition and the penetration of slabs into the lower mantle.

Acknowledgements

This work evolved from calculations done by one of us (H.S.) during a visit at the Scripps Institution of Oceanography, funded by the Deutsche Forschungsgemeinschaft. Fruitful discussions with S. Karato and M. Riedel are highly appreciated. Thoughful reviews of C. Bina, U. Christensen and D. Yuen are gratefully acknowledged. ***[AC]***

References

[1] P. Molnar, D. Freedman, J.S.F. Shih, Length of intermediate and deep seismic zones and temperatures in downgoing slabs of lithosphere, Geophys. J. R. Astron. Soc. 56 (1979) 41–54.

[2] S.H. Kirby, S. Stein, E.A. Okal, D.C. Rubie, Metastable mantle phase transformations and deep earthquakes in subducting oceanic lithosphere, Rev. Geophys. 34 (1996) 261–301.

[3] C.M. Sung, R.G. Burns, Kinetics of high-pressure phase transformations: implications to the evolution of the olivine–spinel transition in the downgoing lithosphere and its consequences on the dynamics of the mantle, Tectonophysics 31 (1976) 1–32.

[4] D.C. Rubie, C.R. Ross, Kinetics of the olivine–spinel transformation in subducting lithosphere: experimental constraints and implications for deep slab processes, Phys. Earth Planet. Inter. 86 (1994) 223–241.

[5] P.C. Burnley, H.W. Green, Faulting associated with the olivine–spinel transformation in Mg_2GeO_4 and its implications for deep-focus earthquakes, J. Geophys. Res. 96 (1991) 425–443.

[6] T. Iidaka, D. Suetsugu, Seismological evidence for metastable olivine inside a subducting slab, Nature 356 (1992) 593–595.
[7] S.W. Roecker, Velocity structure in the Izu-Bonin seismic zone and the depth of the olivine spinel phase transition in the slab, J. Geophys. Res. 90 (1985) 7771–7794.
[8] K.D. Koper, D.A. Wiens, L.M. Dorman, J.A. Hildebrand, S.C. Webb, Modeling the Tonga slab: Can travel time data resolve a metastable olivine wedge?, J. Geophys. Res. in press, 1998.
[9] D.A. Wiens, J.J. McGuire, P.J. Shore, Evidence for transformational faulting from a deep double seismic zone in Tonga, Nature 364 (1993) 790–793.
[10] T. Iidaka, K. Obara, Seismological evidence for the existence of anisotropic zone in the metastable wedge inside the subducting Izu-Bonin slab, Geophys. Res. Lett. 24 (1997) 3305–3308.
[11] E. Ito, H. Sato, Effect of phase transformations on the dynamics of the descending slab, in: Y. Syono, M.H. Manghnani (Ed.), High-Pressure Research: Application to Earth and Planetary Sciences, Geophys. Monogr. 67 (1992) 257–262.
[12] C.R. Bina, Phase transition buoyancy contributions to stresses in subducting lithosphere, Geophys. Res. Lett. 23 (1996) 3563–3566.
[13] C.R. Bina, Patterns of deep seismicity reflect buoyancy stresses due to phase transformations, Geophys. Res. Lett. 24 (1997) 3301–3304.
[14] S. Yoshioka, R. Daessler, D.A. Yuen, Stress fields associated with metastable phase transitions in descending slabs and deep-focus earthquakes, Phys. Earth Planet. Inter. in press, 1998.
[15] H. Schmeling, G.Y. Bussod, Variable viscosity convection and partial melting in the continental asthenosphere, J. Geophys. Res. 101 (1996) 5411–5423.
[16] H. Schmeling, G. Marquart, The influence of second scale convection on the thickness of the continental lithosphere and crust, Tectonophysics 189 (1991) 281–306.
[17] Q. Bai, S.J. Mackwell, D.L. Kohlstedt, High temperature creep of olivine single crystals: Mechanical results for buffered samples, J. Geophys. Res. 96 (1991) 2441–2463.
[18] R. Däßler, D.A. Yuen, S. Karato, M. Riedel, Two-dimensional modeling of thermo-kinetic coupling and the consequences on the phase boundaries of subducting slabs, Phys. Earth. Planet. Inter. 94 (1996) 217–239.
[19] R. Däßler, D.A. Yuen, The effects of phase transition kinetics on subducting slabs, Geophys. Res. Lett. 20 (1993) 2603–2606.
[20] V.S. Solomatov, D.J. Stevenson, Can sharp seismic discontinuities be caused by non-equilibrium phase transformations?, Earth Planet. Sci. Lett. 125 (1994) 267–279.
[21] M. Akaogi, E. Ito, A. Navrotsky, Olivine-modified spinel–spinel transition in the system Mg_2SiO_4–Fe_2SiO_4: Calorimetric measurements, thermochemical calculation and geophysical application, J. Geophys. Res. 94 (1989) 15671–15685.
[22] L. Kerschhofer, C. Dupas, M. Liu, T.G. Sharp, W.B. Durham, D.C. Rubie, Polymorphic transformations between olivine, wadsleyite and ringwoodite: mechanisms of intracrystalline transformation and the role of elastic strain, Mineral. Mag. 62 (1998) 617–638.
[23] M. Liu, L. Kerschhofer, J.L. Mosenfelder, D.C. Rubie, The effect of strain energy on growth rates during the olivine–spinel transformation and implications for olivine metastability in subducting slabs, J. Geophys. Res. in press, 1998.
[24] U.R. Christensen, The influence of trench migration on slab penetration into the lower mantle, Earth Planet. Sci. Lett. 140 (1996) 27–39.
[25] M. Riedel, S. Karato, Grain-size evolution in subducted oceanic lithosphere associated with the olivine–spinel transformation and its effects on rheology, Earth Planet. Sci. Lett. 148 (1997) 27–43.
[26] F.C. Marton, C.R. Bina, S. Stein, D.C. Rubie, Effects of slab mineralogy on subduction rates, Geophys. Res. Lett. in press, 1998
[27] W.A. Bassett, The diamond cell and the nature of the Earth's mantle, Annu. Rev. Earth Planet. Sci. 7 (1979) 357–384.
[28] D.C. Rubie, Mechanisms and kinetics of solid-state reconstructive phase transformations in the Earth's mantle. In: Luth, R.W. (Ed.), Short Course Handbook on Experiments at High Pressure and Applications to the Earth's Mantle, vol. 21, Mineralogical Association of Canada, Edmonton, 1993, pp. 247–303.
[29] R.P. Denlinger, A revised estimate for the temperature structure of the oceanic lithosphere, J. Geophys. Res. 97 (1992) 7219–7222.
[30] C.A. Stein, S. Stein, A model for the global variation in oceanic depth and heat flow with lithospheric age, Nature 359 (1992) 123–129.
[31] C.A. Stein, Heat flow of the earth, in: Global Earth Physics, a Handbook of Physical Constants, AGU Reference Shelf 1, AGU, Washington, 1995, pp. 144–158.
[32] J.G. Sclater, B. Parsons, C. Jaupart, Oceans and continents: similarities and differences in the mechanisms of heat loss, J. Geophys. Res. 86 (1981) 11535–11552.
[33] D.C. Rubie, The olivine spinel transformation and the rheology of subducting lithosphere, Nature 308 (1984) 505–508.